

Research Article

An Adaptive Neural Sliding Mode Controller Design for Autonomous Underwater Vehicle based on Improved Grey Wolf Optimization Algorithm**Mustafa Wassef Hasan* and Nizar Hadi Abbas***University of Baghdad, College of Engineering, Department of Electrical Engineering, Al-Jadriya, Baghdad, Iraq.*

Received 11 February 2022; Accepted 6 May 2022

Abstract

An adaptive neural sliding mode with improved grey wolf optimization (ANSIGWO) controller is proposed in this paper for the autonomous underwater vehicle (AUV) with six degrees of freedom. The proposed ANSIGWO controller is presented to eliminate the environmental disturbances and uncertainties effect leading to trajectory tracking problems. The main principle of the ANSIGWO controller is to estimate both the disturbances and unknown uncertainties of the AUV dynamics and achieve a high precision position of control. In this way, online learning ability is used to deal with both the high nonlinear uncertainty and the time-varying environmental disturbances effect. The outstanding properties of the ANSIGWO controller are evaluated by a comparative analysis between the proposed controller, and other existing works that are quantum behaved particle swarm optimization (QPSO) with model predictive control (MPC), an adaptive neuro-fuzzy sliding mode based genetic algorithm (ANFSGA), and adaptive neuro-fuzzy sliding mode controller (ANFSMC). At the end, the results show that the ANSIGWO controller enhanced the efficiency of path planning by 30.8388%, 43.5245%, and 49.9285% compared to the ANFSGA, QPSO-MPC, and ANFSMC controllers, respectively.

Keywords: AUV, Adaptive neural sliding mode based on improved grey wolf optimization (ANSIGWO), adaptive neuro-fuzzy sliding mode controller (ANFSMC), adaptive neuro-fuzzy sliding based on genetic algorithm (ANFSGA).

1. Introduction

An autonomous underwater vehicle (AUV) is considered one of the several studies that have been discussed during the last decades due to its purposes and applications in different fields such as military applications, pipelining, oceanography and oil and gas industries.

Trajectory tracking of underwater vehicle controller design is deemed a difficult task due to several issues that face the underwater vehicles during their operation, i.e., disturbances issues such as sea currents fluctuation that causes environmental force, nonlinearity, time variance, and modelling parameter acquired difficulty [1].

Several controllers have been used to control the underwater robotic vehicle, such as self-tuning PID [2,3], model-free reinforcement learning algorithm by Wu et al. [4], sliding mode controller [5,6], predictive model controller (MPC) by Steenson et al. [7], adaptive sliding mode controller by Guo et al. [8], swarm AUVs navigation by Leblond et al. [9], nonlinear fractional-order PID by Hasan et al. [10], H-infinity control by Cheng et al. [11]

Different techniques are used to solve the autonomous underwater vehicle problems; one of these techniques is the adaptive mechanism, which is used widely due to its benefit of adjusting system position, reducing system error caused by a different problem, and learning the system dynamics [12–14]. The adaptive mechanism is usually coupled with other techniques or controllers, i.e., Guerrero et al. [15], presents an adaptive observer for trajectory tracking problem of two degrees of freedom underwater vehicle to increase and improved the backstepping and nonlinear (PD) controllers responses under constant disturbances effect. Simultaneously,

Gan et al. [16], proposed a model predictive control based on quantum particle swarm optimization (QPSO) to solve the dynamic trajectory tracking in the three-dimensional environment. Javadi-Moghaddam and Bagheri [17], presents an adaptive neuro-fuzzy sliding mode based on a genetic algorithm (ANFSGA) for tracking control in four degrees of freedom (DOF)s. Lakhekar et al. [18], proposed an adaptive neuro-fuzzy sliding mode control (ANFSMC) for trajectory tracking problems despite the uncertainty and external disturbances so that the depth position tracks the desired trajectory. Khodayari et al. [19] presents a self-adaptive fuzzy PID controller for heading and depth channels.

Motivated by the above analysis, an adaptive neural network based on improved grey wolf optimization controller design is proposed for six degrees of freedom autonomous underwater vehicle. The proposed controller can solve complex AUV system with trajectory tracking problems in the presence of uncertainties and environmental disturbances compared to [17] that present lower performance with four degrees of freedom and compared to [16], which present performance in a three-dimensional environment or that in [18] which will be limited to a specific type of uncertainty and disturbances.

The main contribution of the ANSIGWO is listed as follows:

- The adaptive neural network is used to estimate both the disturbances and uncertainty.
- The improved grey wolf optimization algorithm is used with an adaptive mechanism as an online controller to give the AUV model robustness against uncertainty and external disturbances.

*E-mail address: m.hasan0902@coeng.uobaghdad.edu.iq

ISSN: 1791-2377 © 2022 School of Science, IHU. All rights reserved.

doi:10.25103/jestr.151.13

- By combining both of the adaptive neural networks with the improved grey wolf optimization, the trajectory tracking of the AUV is enhanced.

The ANSIGWO is compared with other existing works related to the same topics with different optimization algorithms based on environmental design workspace path tracking with disturbances area.

The remainder of this work is structured as follows. Section 2 describes the AUV model used in this work. The adaptive neural sliding mode based on improved grey wolf optimization controller design is stated in Section 3. Then, the fundamental result of this work and some numerical simulations to verify the efficiency of the presented controller are proposed in Section 4. At the end, the conclusion part is presented in Section 5.

2. Modelling of Autonomous Underwater Vehicle

The AUVs model [20,21] can be expressed as Body-Fixed Reference (BRF), an Inertial Reference Frame (IRF), or an earth fixed frame. The AUV can be described as translational and rotational components (Suge, Sway, Heave, Roll, Pitch, Yaw), as shown in Fig. (1). AUV dynamics described by vector velocity $v = [X_1, X_2]^T$ where $X_1 = [u, v, w]^T$ which represent linear velocities and $X_2 = [p, q, r]^T$ which represent angular velocities of (Suge, Sway, Heave, Roll, Pitch, Yaw) respectively, while IRF can express as the vector $\eta = [\eta_1, \eta_2]^T$ where $\eta_1 = [x, y, z]^T$ and $\eta_2 = [\varphi, \theta, \psi]^T$ both η_1 and η_2 represents the position and rotational coordinate of the AUV.

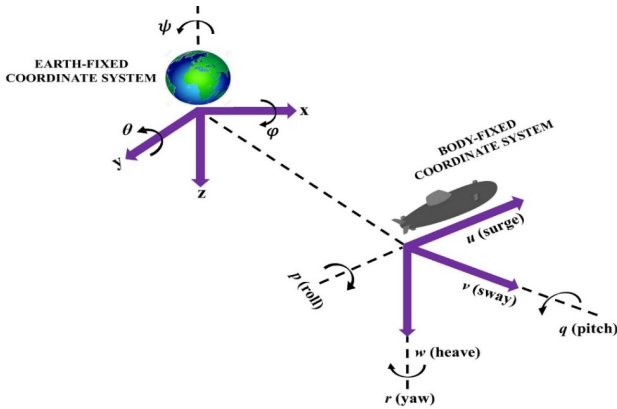


Fig. 1. AUV reference frames.

Vehicle dynamics described by T. I. Fossen (1994) [22] as follows:

$$M\dot{v} + C(v)v + D(v)v + g(\eta) = F_\eta + D \quad (1)$$

where $M \in \mathbb{R}^{6 \times 6}$ is the inertia matrix, $C(v) \in \mathbb{R}^{6 \times 6}$ is the coriolis and centripetal matrix, $D(v) \in \mathbb{R}^{6 \times 6}$ is the hydrodynamic damping of the AUV, $g(\eta) \in \mathbb{R}^6$ is the buoyancy and gravitational vector, $F \in \mathbb{R}^6$ is the torque force applied on the AUV, and $D \in \mathbb{R}^6$ are the disturbances applied on the AUV.

The total AUV disturbances D is given as follows:

$$D = D_{oc} + D_{wa} \quad (2)$$

where D_{oc} and D_{wa} defined as the ocean currents and waves induced moments, respectively.

where D_{oc} are given as follows:

$$D_{oc} = M\dot{v}_r + C(v_r)v_r + D(v_r)v_r + g(\eta) - F_\eta \quad (3)$$

$v_r = v - v_c$, where v_c is the ocean waves velocity.

While D_{wa} are given as follows:

$$D_{wa} = \begin{bmatrix} \sum_{i=1}^M \rho g B L T \cos(\beta) Y_i(t) \\ \sum_{i=1}^M -\rho g B L T \sin(\beta) Y_i(t) \\ 0 \\ 0 \\ 0 \\ \sum_{i=1}^M \frac{1}{24} \rho g B L (L^2 - B^2) \sin(2\beta) Y_i^2(t) \end{bmatrix} \quad (4)$$

where ρ is the water density, B is the breadth of the vessel, T is the draft of the vessel, L is the length of the vessel, β is the encounter angle, and $Y_i(t)$ defined as the wave slope of the wave component i which is defined as follows:

$$Y_i(t) = A m_i \frac{2\pi}{\delta_i} \sin(w_{ei}t + \phi_i) \quad (5)$$

where $A m_i$ is the wave amplitude, w_{ei} is the encounter frequency, δ_i is the wavelength, and ϕ_i is a random phase uniformly distributed and constant with time corresponding to the wave component i . The uncertainty depends on [23,24], where the dynamic uncertainty is inserted with the kinematics model.

Eq. (1) transformed into earth fixed coordinate as follows:

$$M_\eta(\eta)\ddot{\eta} + C_\eta(v, \eta)\dot{\eta} + D_\eta(v, \eta)\dot{\eta} + g_\eta(\eta) = F_\eta(\eta) + D_\eta(t) \quad (6)$$

where $M_\eta(\eta) = J_\eta^{-T} M J_\eta^{-1}$, $C_\eta(\eta) = J_\eta^{-T} [C(v) - M J_\eta^{-1} \dot{J}_\eta] J_\eta^{-1}$, $D_\eta(\eta) = J_\eta^{-T} D(v) J_\eta^{-1}$, $g_\eta = J_\eta^{-T} g(\eta)$, $F_\eta(\eta) = J_\eta^{-T} F_\eta$, and

$$D_\eta(t) = J_\eta^{-T} D(t).$$

Denote $\zeta_1 = \eta$, $\zeta_2 = \dot{\eta}$

Eq. (6) can be transformed as follows:

$$\begin{cases} \dot{\zeta}_1 = \zeta_2 \\ \dot{\zeta}_2 = -M_\eta(\eta)^{-1} C_\eta(v, \eta)\dot{\eta} - M_\eta(\eta)^{-1} D_\eta(v, \eta)\dot{\eta} - M_\eta(\eta)^{-1} g_\eta(\eta) + M_\eta(\eta)^{-1} F_\eta(\eta) + M_\eta(\eta)^{-1} D_\eta(t) \end{cases} \quad (7)$$

Eq. (7) can be expressed as follows:

$$\begin{cases} \dot{\zeta}_1 = \zeta_2 \\ \dot{\zeta}_2 = G(\zeta) + R(\zeta)F_\eta + D(t) \end{cases} \quad (8)$$

where $G(\zeta) = -M_\eta(\eta)^{-1} C_\eta(v, \eta)\dot{\eta} - M_\eta(\eta)^{-1} D_\eta(v, \eta)\dot{\eta} - M_\eta(\eta)^{-1} g_\eta(\eta)$, $R(\zeta) = M_\eta(\eta)^{-1} J_\eta^{-T}$, and $D(t) = M_\eta(\eta)^{-1} D_\eta(t)$.

The uncertainty developed on the system based on [23,24] described as $\dot{U}_s = M_s^{-1}K_s + d_i$, where $\dot{U}_s = [\dot{u} \ \dot{v} \ \dot{w} \ \dot{p} \ \dot{q} \ \dot{r}]^T$, $K_s = [\sum X \ \sum Y \ \sum Z \ \sum K \ \sum M \ \sum N]^T$ defined as the total forces applied on the URV, $d_i = [d_u \ d_v \ d_w \ d_p \ d_q \ d_r]^T$ is the lumped uncertainties that caused by internal noise caused by conductors or joints or may that caused by winds effect, M_s^{-1} described in Appendix A.

3. Adaptive Neural Controller Design

Let the AUV control be represented as follows:

$$\mathfrak{u} = \dot{e} + ce + \hat{F} \tag{9}$$

where $e = \zeta_1^d - \zeta_1$, ζ_1^d is the AUV desired reference trajectory, ζ_1 are the output response of the system and $c = \text{diag}(c1, c2, c3, c4, c5, c6) \in \mathbb{R}^{6 \times 6}$ is a positive diagonal matrix, and \hat{F} defined as the adaptive compensation estimator of both uncertainty and disturbances.

Assumption 1. Assume the (roll, pitch, and yaw) angles are located in the region of $(-\pi < \varphi < \pi)$, $(-\pi < \theta < \pi)$, and $(-\pi < \psi < \pi)$.

Assumption 2. Let the desired signal or trajectory ζ_d of the first-order and second-order derivatives are bounded.

Assumption 3. Let the environmental disturbance $D(t)$ assumed to be a continuous signal and bounded.

It is knowing that one of the most severe problems the URV faces is the uncertainties caused by unknown dynamic parameters [25,26] and disturbances. Both of the uncertainty and disturbances are unpredictable and hard to find in the real world. Thus, using RBF to reduces the computational burden instead of typical techniques used with neural networks as it described by Liu [12]. The RBF consists of three layers (input layer, hidden layer, and output layer). The hidden layer uses Gaussian function as an activation function and describes as follows:

$$W_1(t, \zeta) = \text{diag}(W_{11}(t, \zeta), W_{12}(t, \zeta), W_{13}(t, \zeta), W_{14}(t, \zeta), W_{15}(t, \zeta), W_{16}(t, \zeta)) \tag{15}$$

$$W_2(t, \zeta) = \text{diag}(W_{21}(t, \zeta), W_{22}(t, \zeta), W_{23}(t, \zeta), W_{24}(t, \zeta), W_{25}(t, \zeta), W_{26}(t, \zeta)) \tag{16}$$

Such that, each of the diagonal elements can be represented as follows:

$$W_{1j}(t, \zeta) = A_j + \frac{K_j^2}{4H_j B_j} + \frac{H_j}{B_j} + 2H_j + \frac{8H_j^3}{B_j} + \frac{K_j}{B_j} \tag{17}$$

$$W_{2j}(t, \zeta) = B_j + 4H_j^2 + 2H_j W_{1j} \tag{18}$$

where A_j , H_j , K_j , and B_j are constant numbers with $j = 1, 2, \dots, 6$.

$$N_1(\mathfrak{u}) = |\mathfrak{u}|^{\frac{1}{2}} \text{sgn}(\mathfrak{u}) + \mathfrak{u} \tag{19}$$

$$N_2(\mathfrak{u}) = \frac{1}{2} \cdot \text{sgn}(\mathfrak{u}) + \frac{1}{3} |\mathfrak{u}|^{\frac{1}{2}} \text{sgn}(\mathfrak{u}) + \mathfrak{u} \tag{20}$$

$$h_j = \exp\left(\frac{\|e_i - \pi_j\|}{2b_j^2}\right), j = 1, 2, \dots, 6$$

where e_i is the input vector, π_j and b_j are the mean and standard deviation of the corresponding Gaussian function.

The RBF output is given as follows:

$$y(t) = w_1 h_1 + w_2 h_2 + \dots + w_m h_m = W^T H.$$

where W represents the RBF weights.

Theorem 1. Let the AUV system mentioned in Eq. (1) be transformed into Eq. (6), and if **Assumptions 1-3** are satisfied, then let the URV control law of the closed-loop system proved under AUV control law F_η .

Proof. Consider the AUV mathematical system, let the AUV control law equal to the follows:

$$F_\eta = J^T M_\eta(\eta) \left[\zeta_1^{\ddot{d}} + c\dot{e} - \hat{G}(\zeta) - Q - \hat{D}(t) \right] \tag{10}$$

where $\hat{G}(\zeta)$ is the unknown uncertainty estimator obtained, such that RBF used to approximate the function value as follows:

$$\hat{G}(\zeta) = \hat{W}_1 H(\zeta) = \hat{S}_1 \tag{11}$$

$\hat{D}(t)$ is the unknown disturbances estimator and also obtained by RBF as follows:

$$\hat{D}(t) = \hat{W}_2 H(\zeta) = \hat{S}_2 \tag{12}$$

While

$$Q = -W_1(t, \zeta) \cdot N_1(\mathfrak{u}) + \beta \tag{13}$$

$$\dot{\beta} = -W_2(t, \zeta) \cdot N_2(\mathfrak{u}) \tag{14}$$

The values of $(W_1(t, \zeta), W_2(t, \zeta))$ equal as follows:

The closed-loop system of the AUV can be found from Eq. (9) by taking the time derivative of this equation as follows:

$$\dot{\mathfrak{u}} = \ddot{e} + c\dot{e} + \dot{\hat{F}} \tag{21}$$

where $\ddot{e} = \zeta_1^{\ddot{d}} - \ddot{\zeta}_1$, Eq. (21) can be represented as follows:

$$\dot{\mathfrak{u}} = \zeta_1^{\ddot{d}} - \ddot{\zeta}_1 + c\dot{e} + \dot{\hat{F}} \tag{22}$$

Now, by substituting Eq. (10) into Eq. (22), the following equations are obtained:

$$\dot{\mathfrak{u}} = J^{-T} M_\eta(\eta)^{-1} F_\eta - c\dot{e} + G(\zeta) + Q + \hat{E} - \ddot{\zeta}_1 + c\dot{e} + \dot{\hat{F}} \tag{23}$$

$$\dot{\mu} = J^{-T} M_{\eta}(\eta)^{-1} F_{\eta} - c\dot{e} + \hat{G}(\zeta) + Q + \hat{D}(t) - G(\zeta) - R(\zeta)F_{\eta} - D(t) + c\dot{e} + \hat{F} \quad (24)$$

$$\dot{\mu} = Q + \hat{G}(\zeta) - G(\zeta) + \hat{D}(t) - D(t) + \hat{F} \quad (25)$$

The optimal weights values for function $G(\zeta)$ are approximated and described by Cui et al. [27] as follows:

$$S_1^* = \arg \min_{x_1 \in \Omega} [sup|\hat{G}(\zeta) - G(\zeta)|] \quad (26)$$

The error for the function above is defined and described by Pan and Er [28], Edalati et al. [29] as follows:

$$\lambda_1 = \hat{G}(\zeta|S_1^*) - G(\zeta) \quad (27)$$

Now, the values of the optimal weight for function $D(t)$ are approximated as follows:

$$S_2^* = \arg \min_{x_1 \in \Omega} [sup|\hat{D}(t) - D(t)|] \quad (28)$$

The error for the function above is defined as follows:

$$\lambda_2 = \hat{D}(t|S_2^*) - D(t) \quad (29)$$

$$\dot{\mu} = Q + [\hat{G}(\zeta) - \hat{G}(\zeta|S_1^*) + \lambda_1] + [\hat{D}(t) - \hat{D}(t|S_2^*) + \lambda_2] + \hat{F} \quad (30)$$

$$\dot{\mu} = Q + [(\hat{S}_1 - S_1^*)^T + \lambda_1] + [(\hat{S}_2 - S_2^*)^T + \lambda_2] + \hat{F} \quad (31)$$

Now, let the adaptive law \hat{F} equal to the follows:

$$\dot{\hat{F}} = -\frac{1}{\delta} [(\hat{S}_1 - S_1^*)^T \hat{\Delta}_1 + (\hat{S}_2 - S_2^*)^T \hat{\Delta}_2] \quad (32)$$

$$\begin{aligned} \dot{\mu} &= Q - \frac{1}{\delta} [(\hat{S}_1 - S_1^*)^T (\hat{\Delta}_1 - \delta)] - \frac{1}{\delta} [(\hat{S}_2 - S_2^*)^T (\hat{\Delta}_2 - \delta)] \\ &+ \lambda_1 + \lambda_2 \end{aligned} \quad (33)$$

$$\dot{\mu} = Q - \left[\frac{1}{\delta} \quad \frac{1}{\delta} \right] \begin{bmatrix} (\hat{S}_1 - S_1^*)^T (\hat{\Delta}_1 - \delta) \\ (\hat{S}_2 - S_2^*)^T (\hat{\Delta}_2 - \delta) \end{bmatrix} + \lambda_1 + \lambda_2 \quad (34)$$

$$\dot{\mu} = Q - [Y(\hat{S} - S^*)^T (\hat{\Delta} - \delta)]^T + \lambda_1 + \lambda_2 \quad (35)$$

Next, by using the IGWO [10], the adaptive parameter $\hat{\Delta}$ can reach the value of $\hat{\Delta} = \delta$, thus $\dot{\mu}$ equal to the following equation:

$$\dot{\mu} = Q + \lambda_1 + \lambda_2 \quad (36)$$

$$\dot{X} = \begin{bmatrix} N_1(z_1) \cdot \left(-W_1 \cdot \left(|z_1|^{\frac{1}{2}} \operatorname{sgn}(z_1) + z_1 \right) + z_2 \right) \\ -W_2 \cdot \left(1/2 \cdot \operatorname{sgn}(z_1) + 1/3 |z_1|^{\frac{1}{2}} \operatorname{sgn}(z_1) + z_1 \right) + \frac{d}{dt} \lambda_1 + \frac{d}{dt} \lambda_2 \end{bmatrix} \quad (42)$$

Now, using regions (1 and 2) in Eq. (42), the following vector is presented:

Now, by taking the integration of Eq. (14) and by substituting it in Eq. (13) and then substitute the result in Eq. (36), gives the following equation:

$$\begin{aligned} \mu &= -W_1(t, \zeta) \cdot N_1(\mu) - W_2(t, \zeta) \int_0^t N_2(\mu(\tau)) d\tau + \lambda_1 \\ &+ \lambda_2 \end{aligned} \quad (37)$$

Let

$$z_{1j} = \mu_j$$

$$z_{2j} = -W_{2j} \int_0^t N_2(\mu_j(\tau)) d\tau + \lambda_{j1} + \lambda_{j2} \quad (38)$$

Now, by taking the time derivative for both equations above and then represent it in the scalar form for better clarify the following equation is obtained:

$$\begin{aligned} \dot{z}_1 &= -W_1 \cdot \left(|z_1|^{\frac{1}{2}} \operatorname{sgn}(z_1) + z_1 \right) + z_2 \\ \dot{z}_2 &= -W_2 \cdot \left(1/2 \cdot \operatorname{sgn}(z_1) + 1/3 |z_1|^{\frac{1}{2}} \operatorname{sgn}(z_1) + z_1 \right) \\ &+ \frac{d}{dt} \lambda_1 + \frac{d}{dt} \lambda_2 \end{aligned} \quad (39)$$

From **Assumption 2** and **Assumption 3**, the time derivative of the λ_1 is exists everywhere in the bounded region.

Then region (1) is equal to the follows:

$$\|\dot{\lambda}_{j1}(t)\|_2 \leq M_j \|N_2(\mu)\|_2, j = 1, 2, \dots, 6$$

Such that $M_j \geq 0$ and the same assumptions (2 and 3) can be developed on λ_2 such that region (2) is equal to the follows:

$$\|\dot{\lambda}_{j2}(t)\|_2 \leq S_j \|N_2(\mu)\|_2, j = 1, 2, \dots, 6$$

Now, let the following candidate Lyapunov function is presented

$$V = X^T P X \quad (40)$$

Next, let the vector X equal to the follows:

$$X = \begin{bmatrix} N_1(z_1) \\ z_2 \end{bmatrix} \triangleq \begin{bmatrix} |z_1|^{\frac{1}{2}} \operatorname{sgn}(z_1) + z_1 \\ z_2 \end{bmatrix} \quad (41)$$

Knowing that ($\dot{X} = AX$) and by taking the derivative of vector $X \xrightarrow{yields} \dot{X} = \begin{bmatrix} N_1(z_1) \cdot \dot{z}_1 \\ \dot{z}_2 \end{bmatrix}$

$$\dot{X} = \begin{bmatrix} N_1 \dot{z}_1 \cdot \left(-W_1 \cdot \left(|z_1|^{\frac{1}{2}} \text{sgn}(z_1) + z_1 \right) + z_2 \right) \\ -W_2 \cdot \left(\frac{1}{2} \cdot \text{sgn}(z_1) + \frac{1}{3} |z_1|^{\frac{1}{2}} \text{sgn}(z_1) + z_1 \right) + SN_2(z_1) + MN_2(z_1) \end{bmatrix} \quad (43)$$

By taking the time derivative of $N_1(z_1)$ the following equation is presented:

$$N_1 \dot{z}_1 = \frac{1}{2} \frac{1}{|z_1|^{\frac{1}{2}}} + 1 \quad (44)$$

Knowing that if Eq. (44) is multiplied by $N_1(z_1)$ the following equation is presented:

$$\left(\frac{1}{2} \frac{1}{|z_1|^{\frac{1}{2}}} + 1 \right) * \left(|z_1|^{\frac{1}{2}} \text{sgn}(z_1) + z_1 \right) \xrightarrow{\text{yields}} \left(\frac{1}{2} \text{sgn}(z_1) + \frac{1}{2} \frac{z_1}{|z_1|^{\frac{1}{2}}} + |z_1|^{\frac{1}{2}} \text{sgn}(z_1) + z_1 \right) \quad (45)$$

$$\dot{X} = \begin{bmatrix} N_1 \dot{z}_1 \cdot \left(-W_1 \cdot \left(|z_1|^{\frac{1}{2}} \text{sgn}(z_1) + z_1 \right) + z_2 \right) \\ -W_2 \cdot N_1 \dot{z}_1 \cdot N_1(z_1) + SN_1 \dot{z}_1 \cdot N_1(z_1) + MN_1 \dot{z}_1 \cdot N_1(z_1) \end{bmatrix} \quad (48)$$

Now, taking the time derivative of Eq. (40) led to the following equation

$$\dot{V} = \dot{X}^T P X + X^T P \dot{X} \quad (49)$$

$$\dot{V} = N_1 \dot{z}_1 \cdot X^T (A^T P + P A) X \quad (50)$$

Where

$$A = \begin{bmatrix} \frac{\partial \dot{X}_1}{\partial z_1} & \frac{\partial \dot{X}_1}{\partial z_2} \\ \frac{\partial \dot{X}_2}{\partial z_1} & \frac{\partial \dot{X}_2}{\partial z_2} \end{bmatrix} \xrightarrow{\text{yields}} \begin{bmatrix} -W_1 & 1 \\ -(W_2 - S - M) & 0 \end{bmatrix} \quad (51)$$

where P is chosen to satisfy the positive definite condition $P > 0$ thus, let be equal to

$$P = \begin{bmatrix} 5\gamma^2 & 1.5\gamma \\ 1.5\gamma & 2 \end{bmatrix} > 0 \quad (52)$$

where γ any positive number.

where $A^T P + P A < 0$, thus $L > 0$ is symmetric and

$A^T P + P A = -L$, then Eq. (50) can be written as follows:

$$\dot{V} = -N_1 \dot{z}_1 \cdot X^T L X \quad (53)$$

Next, by using the following formula to solve the candidate Lyapunov candidate solution

$$\lambda_{\min}(P) \|X\|_2 \leq X^T P X \leq \lambda_{\max}(P) \|X\|_2 \quad (54)$$

where $\|X\|_2$ is the norm of X

$$\dot{V} = -N_1 \dot{z}_1 \cdot X^T L X \leq -1.5 \gamma N_1 \dot{z}_1 \cdot X^T L X \quad (55)$$

where

$$\text{sgn}(z_1) = \begin{cases} 1 & \text{if } z_1 > 0 \\ 0 & \text{if } z_1 = 0 \\ -1 & \text{if } z_1 < 0 \end{cases} \quad (46)$$

$$\text{sgn}(z_1) = \frac{z_1}{|z_1|} \text{ except } (z_1 = 0) \quad (47)$$

For $(z_1 > 0)$ and by substitute Eq. (47) into Eq. (45), the result will equal to $N_2(z_1)$ in other words $N_2(z_1) = N_1 \dot{z}_1 \cdot N_1(z_1)$ in Eq. (43) and,

$$\dot{V} = -1.5 \gamma \left(\frac{1}{2} \frac{1}{|z_1|^{\frac{1}{2}}} + 1 \right) X^T L X \quad (56)$$

$$\dot{v} = -a_1 v - a_2 v^{\frac{1}{2}} \quad v(0) \geq 0 \quad (57)$$

$$a_1 = \frac{\gamma \lambda_{\min}^{1/2}}{\lambda_{\max}(P)}, \quad a_2 = \frac{1.5\gamma}{\lambda_{\max}(P)}$$

The solution converges exponentially in the finite time towards the origin.

The system design represented, as shown in Fig. (2) below,

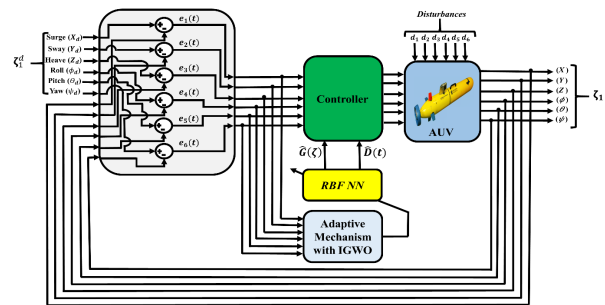


Fig. 2. The proposed system design.

4. Results and Discussion

This section discusses the main reason to develop the IGWO [10] with the adaptive neural sliding (ANS) mode controller, where a comparative analysis of the IGWO is done with slime mold algorithm (SMA) by Li et al. [30], genetic algorithm (GA) by Rebouças et al. [31], particle swarm optimization (PSO) by Isiet and Gadala [32], and grasshopper optimization (GSO) by Saremi et al. [33]. The simulation of the results was done using MATLAB R2018b on a personal computer that has a processor of (Intel(R) Core(TM) i7-7700HQ CPU @

2.80GHz (8 CPUs), ~2.8GHz), and memory of (16 GB RAM).

The first analysis procedure of the IGWO with SMA, GA, PSO, and GSO depend on obtaining the total cost function along with a different number of population (npop) for each algorithm to get the best operation properties for each algorithm. At first, we need to define which cost function is used with work; thus, the following cost function is used by Abbas and Sami [34] and have been used in this research also:

$$\begin{aligned}
 \text{Cost Function}_{ANS-(IGWO-SMA-GA-PSO-GSO)} &= \int_0^t (\zeta_1^d - \zeta_1)^2 d\tau + \int_0^t |\zeta_1^d - \zeta_1| d\tau \\
 &+ \frac{1}{4} Mp \quad (58)
 \end{aligned}$$

where, $Mp = \frac{\zeta_1^d - \zeta_1}{\zeta_1} \times 100\%$, $ISE = \int_0^t (\zeta_1^d - \zeta_1)^2 d\tau$, and $IAE = \int_0^t |\zeta_1^d - \zeta_1| d\tau$.

The maximum peak Mp overshoot used due to its characteristics of decay the response cycle time of the proposed controller (ANS), the integrated square error (ISE) used due to its properties of making the responses fast enough to track the original AUV trajectory, and the integrated absolute error (IAE) were used to eliminate the high oscillation produced by the (ISE).

To proceed with the first analysis procedure and to get the best population number of each algorithm with the ANS controller, we simulate each algorithm for (30) running simulations for population numbers of (20), (25), and (30). Then by taking the average distribution of the collected total cost value of each algorithm alongside each of the given population numbers, Fig. (3) below is obtained. Fig. (3) below represents a box plot of the distribution cost value of each optimization algorithm.

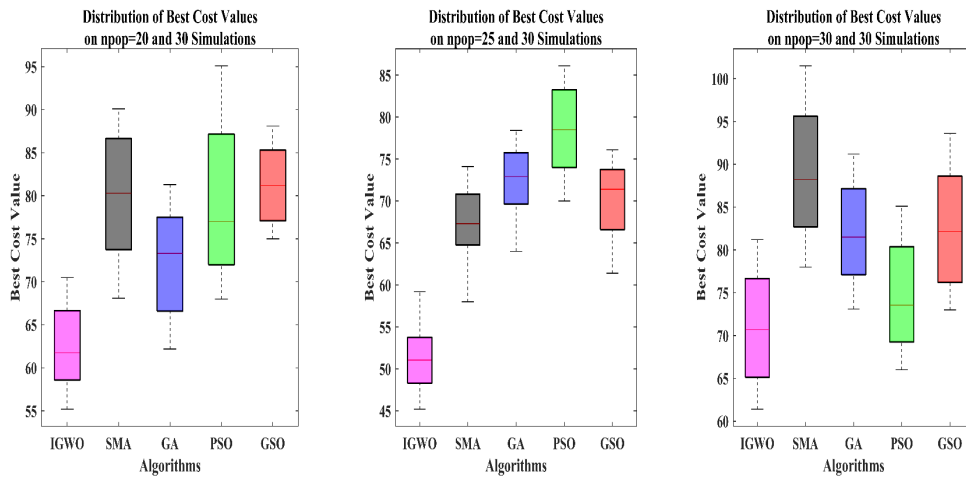


Fig. 3. Average distribution cost value with a different number of populations.

Fig. (3) above show that the IGWO act better with (25) npop as the lowest distribution cost value is presented. At the same time, the PSO algorithm acts better with (30) npop, the GA present better performance with (20) npop, the (SMA) present better performance with (25) npop, and the GSO act better with (25) npop.

Now, each of the optimization algorithms, IGWO, SMA, GA, PSO, and GSO, are operating for a complete running of

iterations; each complete running represents an average cost value of (30) simulation with npop of (25, 25, 20, 30, and 25) for IGWO, SMA, GA, PSO, and GSO respectively. Table 1 and Fig. (4) represents the collected average best cost results versus the number of iteration for each of the optimization algorithms.

Table 1. Average best cost values versus the number of iterations.

SI. No.	Simulation				
	IGWO	SMA	GA	PSO	GSO
1	497.6930	521.4729	520.5839	518.5003	519.4789
50	271.2343	307.4638	304.6432	299.1029	300.2005
100	250.0369	267.5673	260.9743	242.0023	255.9912
150	207.1003	248.6288	240.2234	217.5074	230.0591
200	145.5402	180.5638	170.1375	154.3406	165.5921
250	124.6221	148.5832	145.4732	132.6896	138.6332
280	124.2666	145.0385	138.1377	130.2643	135.1777
310	65.1345	60.4992	80.4563	70.3221	72.6543
340	45.2411	56.3221	55.3442	52.5332	54.4322
370	45.6432	49.1345	51.3454	52.2542	54.2664

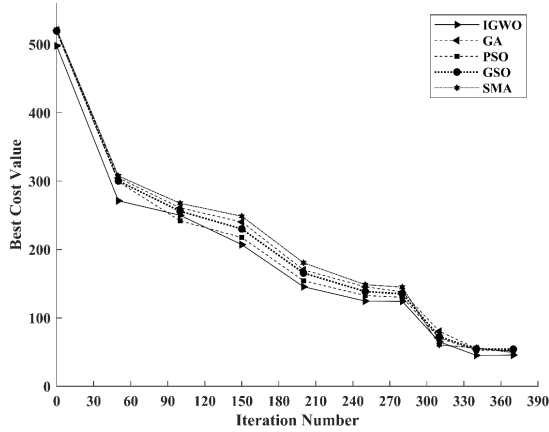


Fig. 4. Average best cost values versus the number of iterations.

The second procedure is to develop the AUV desired trajectory for the ANSIGWO controller, as follows:

$$X_d = 4 * \cos\left(\frac{\pi}{10} * t\right) \tag{59}$$

$$Y_d = 3 * \sin\left(\frac{\pi}{5} * t\right) \tag{60}$$

$$Z_d = u(t) \tag{61}$$

where $u(t)$ is step input, while (t) is the simulation time which equals to $t = 20 \text{ sec}$, the desired roll angle assumed to be $(\varphi_d = \pi/3)$, while the desired pitch angle assumed to be $(\theta_d = \pi/4)$. Finally, the desired yaw angle is assumed to be $(\psi_d = \pi/3.5)$.

The ANSIGWO controller performance is evaluated by a comparative analysis with other existing works, which are quantum behaved particle swarm optimization (QPSO) with model predictive control (MPC) [16], an adaptive neuro-fuzzy sliding mode based genetic algorithm (ANFSGA) [17], and adaptive neuro-fuzzy sliding mode controller (ANFSMC) [18]. Fig. (5) below show the collected results for proposed controllers.

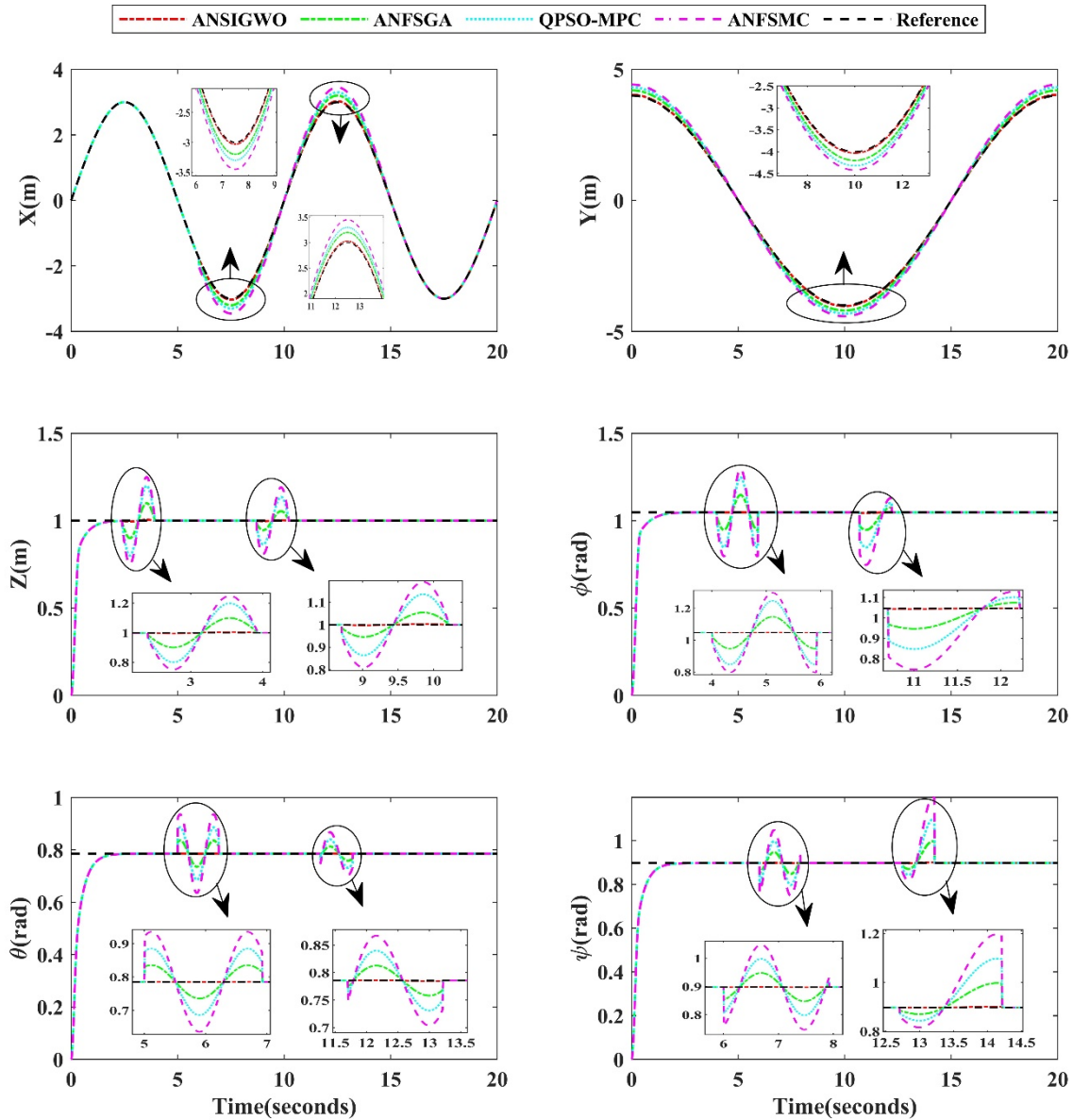


Fig. 5. Trajectory tracking of the AUV for the (ANSIGWO, QPSO-MPC, ANFSGA, and ANFSMC).

Fig. (5) above show clearly that the ANSIGWO controller presents the best performance to reject the disturbances and uncertainties effect compared to QPS-MPC, ANFSGA, and ANFSMC controllers. For better understanding, we proposed bathymetry data [35] used widely to represent the ocean and coastal trajectories for ships and underwater vehicles. The bathymetry data is selected and created depending on the latitude and longitude of the following coordinate region (*west = 48°, east = 52°, south = 29°, north = 31°*). Fig. (6) below show the AUV path planning for the proposed controllers that represents the X and Y responses of Fig. (5).

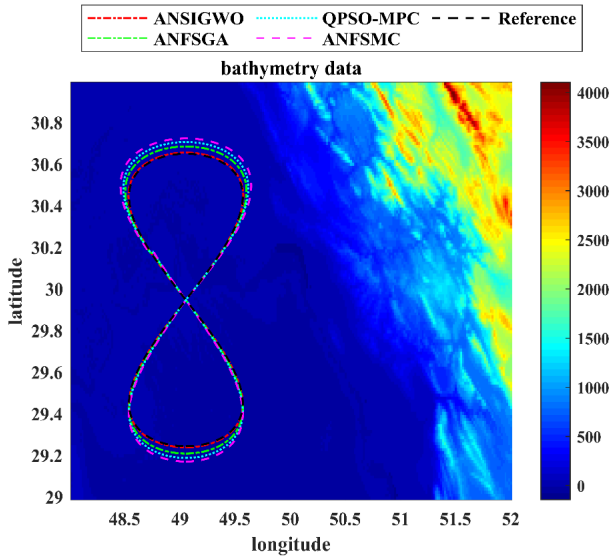


Fig. 6. Path planning of the AUV for the (ANSIGWO, QPSO-MPC, ANFSGA, and ANFSMC) controllers using bathymetry data.

Fig. (6) above shows that the ANSIGWO controller presents the best path planning for tracking the reference signal under ocean currents and wind moments compared to the other controllers. The ANFSMC presents the worst path planning for tracking the reference signal, while the QPSO-MPC presents the best path planning than the ANFSMC, while the ANFSGA presents better performance QPSO-MPC but worst of ANSIGWO.

A computer-aided design (CAD) [36] has been done to create a moving AUV animation along a straight line path planning to evaluate the performance of the ANSIGWO controller across different trajectories with disturbances and uncertainties effects. Fig. (7) below represent the collected results for a straight-line trajectory performance for the ANSIGWO, ANFSGA, QPS-MPC, and ANFSMC controllers.

The results in Fig. (7) indicate that the ANSIGWO controller presents the best path planning trajectory with no effect for each disturbance and uncertainty compared to the ANFSGA, QPS-MPC, and ANFSMC.

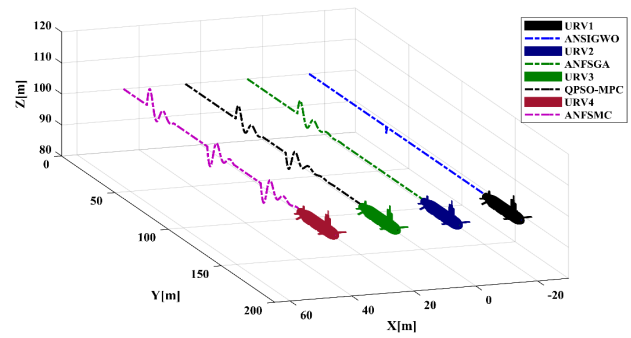


Fig. 7. Path planning of the AUV CAD design for the (ANSIGWO, QPSO-MPC, ANFSGA, and ANFSMC) controllers.

Now another path planning trajectory is proposed to evaluate the performance of the proposed controllers based on the following mathematical equation:

$$X_d = 0.05(100 + 10 \cos(36t/50)) \cos(6t/50) \quad (62)$$

$$Y_d = 0.05(100 + 10 \cos(36t/50)) \sin(6t/50) \quad (63)$$

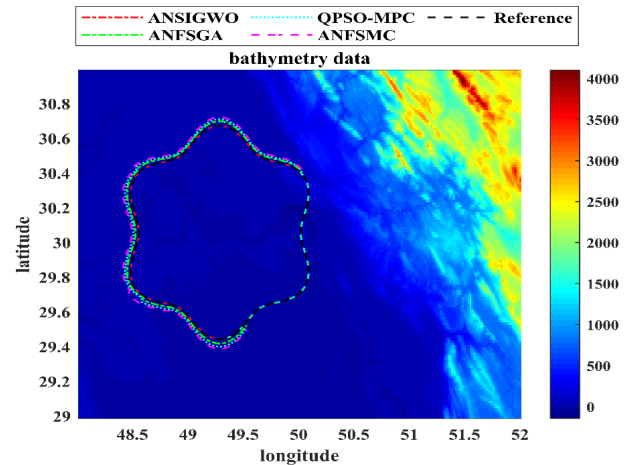


Fig. 8. Path planning of the AUV for the (ANSIGWO, QPSO-MPC, ANFSGA, and ANFSMC) controllers using bathymetry data.

As before, Fig. (8) above shows that the ANSIGWO controller presents the best path planning for tracking the reference signal compared to the ANFSMC, which presents the worst path planning for tracking the reference signal, while the QPSO-MPC presents the best path planning than the ANFSMC, while the ANFSGA presents better performance QPSO-MPC but worst of ANSIGWO.

At the end, the ANSIGWO, ANFSGA, QPSO-MPC, and ANFSMC controllers were also compared using numerical simulations based on taking the average cost value of eight samples. Such that each sample represents a complete running of the proposed controllers. Table 2 and Fig. (9) below demonstrate the results of the average cost function obtained for the selected controllers.

Table 2. Average cost function results for ANSIGWO, ANFSGA, QPSO-MPC and ANFSMC controllers.

Samples Number	ANSIGWO	ANFSGA	QPSO-MPC	ANFSMC
1	45.0399	65.3642	80.1043	90.1938
2	45.1300	65.2405	79.2539	89.8726
3	45.0002	65.0130	79.3002	90.2000
4	44.9201	65.2201	80.1029	90.3330
5	45.1030	64.8013	80.1102	89.5649
6	45.0999	65.4403	79.0005	90.2940
7	44.9987	64.9220	80.2748	89.1348

8	45.1155	65.1110	80.0192	90.1935
Average	45.0509	65.1390	79.7707	89.9733

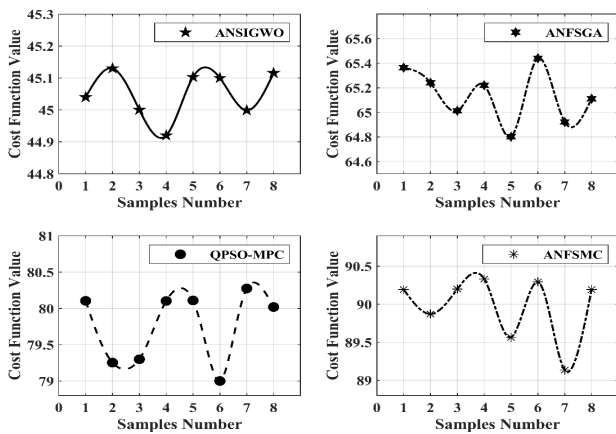


Fig. 9. Average cost function results for ANSIGWO, ANFSGA, QPSO-MPC and ANFSMC controllers.

The enhancement between each controller measured by the following formula [34]:

$$EP]_{Controller A over Controller B} = \left(1 - \frac{OF]_A}{OF]_B}\right) \times 100\% \quad (64)$$

where EP explained as the enhancement percentage of the AUV, while OF is defined as the objective function value of the selected controller.

The enhancement of the ANSIGWO compared to the ANFSGA controller are measured as follows:

$$EP]_{ANSIGWO}^{ANFSGA} = \left(1 - \frac{45.0509}{65.1390}\right) \times 100\% = 30.8388\%$$

The enhancement of the ANSIGWO compared to the QPSO-MPC controller are measured as follows:

$$EP]_{ANSIGWO}^{QPSO-MPC} = \left(1 - \frac{45.0509}{79.7707}\right) \times 100\% = 43.5245\%$$

The enhancement of the ANSIGWO compared to the ANFSMC controller are measured as follows:

$$EP]_{ANSIGWO}^{ANFSMC} = \left(1 - \frac{45.0509}{89.9733}\right) \times 100\% = 49.9285\%$$

5. Conclusions

This paper presents an adaptive neural sliding mode based on an improved grey wolf optimization controller for an autonomous underwater vehicle to solve the path trajectory tracking problem in the underwater vehicle under the model uncertainty and external disturbances. Online learning ability with the adaptive mechanism is provided using an improved grey wolf optimization. The ANSIGWO controller is designed to reduce the impact of the uncertainties and environmental disturbances on the AUV system; afterwards, it was evaluated by comparing the proposed controller with other existing works. The results show that the ANSIGWO controller enhanced the efficiency of path planning by 30.8388%, 43.5245%, and 49.9285% compared to the ANFSGA, QPSO-MPC, and ANFSMC controllers, respectively.

Acknowledgments

Our thanks to all who help us to complete this work.

This is an Open Access article distributed under the terms of the Creative Commons Attribution License.



References

- Zhao, S., Yuh, J. "Experimental study on advanced underwater robot control". *IEEE Trans Robot.* 21, 2005, pp. 695–703.
- Dong, E., Guo, S., Lin, X., Li, X., Wang, Y. "A neural network-based self-tuning PID controller of an autonomous underwater vehicle". In: *2012 IEEE International Conference on Mechatronics and Automation*, 2012, pp. 898–903. <https://doi.org/10.1109/ICMA.2012.6283262>.
- Hernández-Alvarado, R., García-Valdovinos, L. G., Salgado-Jiménez, T., Gómez-Espinoza, A., Fonseca-Navarro, F. "Neural network-based self-tuning PID control for underwater vehicles". *Sensors*, 16(9), 2016, p. 1429. <https://doi.org/10.3390/s16091429>.
- Wu, H., Song, S., You, K., Wu, C. "Depth Control of Model-Free AUVs via Reinforcement Learning". *IEEE Transactions on Systems, Man, and Cybernetics: Systems*, 49(12), 2019, pp. 2499–2510. <https://doi.org/10.1109/TSMC.2017.2785794>.
- Joe, H., Kim, M., Yu, S. cheol. "Second-order sliding-mode controller for autonomous underwater vehicle in the presence of unknown disturbances". *Nonlinear Dynamics*, 78(1), 2014, pp. 183–196. <https://doi.org/10.1007/s11071-014-1431-0>.
- Kim, D., Choi, H. S., Kim, J. Y., Park, J. H., Tran, N. H. "Trajectory generation and sliding-mode controller design of an underwater vehicle-manipulator system with redundancy". *International Journal of Precision Engineering and Manufacturing*, 16(7), 2015, pp. 1561–1570. <https://doi.org/10.1007/s12541-015-0206-y>.
- Stenson, L. V., Wang, L., Phillips, A. B., Turnock, S. R., Furlong, M. E., Rogers, E. "Experimentally verified depth regulation for AUVs using constrained model predictive control". *IFAC Proceedings Volumes*, 47(3), 2014, pp. 11974–11979. <https://doi.org/10.3182/20140824-6-za-1003.01497>.
- Guo, Y., Qin, H., Xu, B., Han, Y., Fan, QY., Zhang, P. "Composite learning adaptive sliding mode control for AUV target tracking". *Neurocomputing*, 351, 2019, pp. 180–186. <https://doi.org/10.1016/j.neucom.2019.03.033>.
- Leblond I, Tauvry S, Pinto M. Sonar image registration for swarm AUVs navigation: Results from SWARMS project. *Journal of Computational Science*, 36, 2019, p. 101021. <https://doi.org/10.1016/j.jocs.2019.07.008>.
- Hasan, M.W., Abbas, N. H. "An improved swarm intelligence algorithms-based nonlinear fractional order-PID controller for a trajectory tracking of underwater vehicles". *TELKOMNIKA*, 18(6), 2020, pp. 3173–3183. <https://doi.org/10.12928/telkomnika.v18i6.16282>.
- Cheng, X. qin., Qu, J. yuan., Yan, Z. ping., Bian, X. qian. "H ∞ robust fault-tolerant controller design for an autonomous underwater vehicle's navigation control system". *Journal of Marine science and Application*, 9(1), 2010, pp. 87–92. <https://doi.org/10.1007/s11804-010-8052-x>.
- Liu, J. *Intelligent control design and MATLAB simulation*, (2017). <https://doi.org/10.1007/978-981-10-5263-7>.
- Liu J, Wang X. *Advanced sliding mode control for mechanical systems*. Springer; 2012.
- Ismael SA, Al-jebory KM. *Adaptive Fuzzy System Modeling Abstract : 1 Introduction 2 Adaptive Fuzzy Systems 2014:1–11*.
- Guerrero, J., Torres, J., Creuze, V., Chemori, A. "Adaptive disturbance observer for trajectory tracking control of underwater vehicles". *Ocean Engineering*, 200, 2020, pp. 107080. <https://doi.org/10.1016/j.oceaneng.2020.107080>.
- Gan, W., Zhu, D., Ji, D. "QPSO-model predictive control-based

approach to dynamic trajectory tracking control for unmanned underwater vehicles". *Ocean Engineering*, 158, 2018, pp. 208–220. <https://doi.org/10.1016/j.oceaneng.2018.03.078>.

17. Javadi-Moghaddam, J., Bagheri, A. "An adaptive neuro-fuzzy sliding mode based genetic algorithm control system for under water remotely operated vehicle". *Expert Systems with Applications*, 37(1), 2010, pp. 647–660. <https://doi.org/10.1016/j.eswa.2009.06.015>.
18. Lakhekar, G. V., Waghmare, L. M., Vaidyanathan, S. "Diving autopilot design for underwater vehicles using an adaptive neuro-fuzzy sliding mode controller". In: *Advances and applications in nonlinear control systems*, Springer; 2016, pp. 477–503.
19. Khodayari, M. H., Balochian, S. "Modeling and control of autonomous underwater vehicle (AUV) in heading and depth attitude via self-adaptive fuzzy PID controller". *Journal of Marine Science and Technology*, 20(3), 2015, pp. 559–578.
20. Shen, C., Shi, Y., Buckham, B. "Lyapunov-based model predictive control for dynamic positioning of autonomous underwater vehicles". In: *2017 IEEE International Conference on Unmanned Systems (ICUS)*, 2018-Janua, pp. 588–593. <https://doi.org/10.1109/ICUS.2017.8278413>.
21. Fischer, N., Bhasin, S., Dixon, W. E. "Nonlinear control of an autonomous underwater vehicle: A RISE-based approach". In: *Proceedings of the 2011 American Control Conference*, 2011, pp. 3972–3977. <https://doi.org/10.1109/acc.2011.5990958>.
22. Fossen, TI. *Guidance and control of ocean vehicles*, Wiley, New York, (1994).
23. Zheng, Z., Ruan, L., Zhu, M. "Output-constrained tracking control of an underactuated autonomous underwater vehicle with uncertainties". *Ocean Engineering*, 175, 2019, p.p 241–250. <https://doi.org/10.1016/j.oceaneng.2019.02.023>.
24. Fossen, TI. *Handbook of Marine Craft Hydrodynamics and Motion Control*. (2011). <https://doi.org/10.1002/9781119994138>.
25. Liang, X., Qu, X., Wan, L., Ma, Q. "Three-Dimensional Path Following of an Underactuated AUV Based on Fuzzy Backstepping Sliding Mode Control". *International Journal of Fuzzy Systems*, 20(2), 2018, 640–649. <https://doi.org/10.1007/s40815-017-0386-y>.
26. Gao, Z., Guo, G. "Adaptive formation control of autonomous underwater vehicles with model uncertainties". *International Journal of Adaptive Control and Signal Processing*, 32, 2018, pp. 1067–1080. <https://doi.org/10.1002/acs.2886>.
27. Cui, J., Zhao, L., Yu, J., Lin, C., Ma, Y. "Neural network-based adaptive finite-time consensus tracking control for multiple autonomous underwater vehicles". *IEEE Access*, 7, 2019, pp. 33064–33074. <https://doi.org/10.1109/ACCESS.2019.2903833>.
28. Pan, Y., Er, M. J. "Enhanced adaptive fuzzy control with optimal approximation error convergence". *IEEE Transactions on Fuzzy Systems*, 21(6), 2013, pp. 1123–1132. <https://doi.org/10.1109/TFUZZ.2013.2244899>.
29. Edalati, L., Sedigh, A. K., Shooredeli, M. A., Moarefianpour, A. "Adaptive fuzzy dynamic surface control of nonlinear systems with input saturation and time-varying output constraints". *Mechanical Systems and Signal Processing*, 100, 2018, pp. 311–329. <https://doi.org/10.1016/j.ymssp.2017.07.036>.
30. Li, S., Chen, H., Wang, M., Heidari, A. A., Mirjalili, S. "Slime mould algorithm: A new method for stochastic optimization". *Future Generation Computer Systems*, 111, 2020, pp. 300–323. <https://doi.org/10.1016/j.future.2020.03.055>.
31. Rebouças, Filho. P. P., Suane, S. P., Praxedes, V. N., Hemanth, J., de Albuquerque, V. H. C. "Control of singularity trajectory tracking for robotic manipulator by genetic algorithms". *Journal of computational science*, 30, 2019, pp. 55–64. <https://doi.org/10.1016/j.jocs.2018.11.006>.
32. Isiet, M., Gadala, M. "Sensitivity analysis of control parameters in particle swarm optimization". *Journal of Computational Science*, 41, 2020, pp. 101086. <https://doi.org/10.1016/j.jocs.2020.101086>.
33. Saremi, S., Mirjalili, S., Lewis, A. Grasshopper Optimisation Algorithm: Theory and application. *Advances in Engineering Software*, 105, 2017, pp. 30–47. <https://doi.org/10.1016/j.advengsoft.2017.01.004>.
34. Abbas, N. H., Sami, A. R. "Tuning of PID controllers for quadcopter system using hybrid memory based gravitational search algorithm–particle swarm optimization". *International Journal of Computer Applications*, 172(04), 2017, pp. 9–18.
35. Ma, T., Li, Y., Wang, R., Cong, Z., Gong, Y. "AUV robust bathymetric simultaneous localization and mapping". *Ocean Engineering*, 166, 2018, pp. 336–49.
36. Aras, M. S., Zhe, K. L., Aripin, M. K., Chaing, T. P., Shah, H. N., Khamis, A., Nordin, N., Rashid, M. Z. "Design analysis and modelling of autonomous underwater vehicle (AUV) using CAD". (2019).
37. Prestero, T. *Verification of a Six-Degree of Freedom Simulation Model*, Massachusetts Inst Technol (2001).

Appendix A

The following matrix represents the kinematic equation used in Eq. (A.1)

$$M_s = \begin{bmatrix} m - X_{\dot{u}} & 0 & 0 & 0 & mz_g & -my_g \\ 0 & m - Y_{\dot{v}} & 0 & -mz_g & 0 & mx_g - Y_{\dot{r}} \\ 0 & 0 & m - Z_{\dot{w}} & my_g & -mx_g - Z_{\dot{q}} & 0 \\ 0 & -mz_g & my_g & I_{xx} - K_{\dot{p}} & 0 & 0 \\ mz_g & 0 & -mx_g - M_{\dot{w}} & 0 & I_{yy} - M_{\dot{q}} & 0 \\ -my_g & mx_g - N_{\dot{v}} & 0 & 0 & 0 & I_{zz} - N_{\dot{r}} \end{bmatrix} \quad (A.1)$$

The total kinematic force is explained in the following vector:

$$k_s = \left[\sum X \quad \sum Y \quad \sum Z \quad \sum K \quad \sum M \quad \sum N \right]^T$$

where

$$\sum X = X_{u|u}|u|u| + X_{wq}wq + X_{vr}vr + X_{\dot{u}}\dot{u} + X_{qq}qq + X_{rr}rr + X_{prop} + X_{HS}$$

$$\sum Y = Y_{v|v}|v|v| + Y_{wp}wp + Y_{ur}ur + Y_{\dot{v}}\dot{v} + Y_{pq}pq + Y_{\dot{r}}\dot{r} + Y_{r|r}|r|r| + Y_{uv}uv + Y_{uu\delta_r}u^2\delta_r + Y_{HS}$$

$$\sum Z = Z_{w|w}|w|w| + Y_{wp}wp + Z_{rp}rp + Z_{\dot{w}}\dot{w} + Z_{vp}vp + Z_{\dot{q}}\dot{q} + Z_{q|q}|q|q| + Z_{uq}uq + Z_{uu\delta_s}u^2\delta_s + Z_{HS}$$

$$\sum K = K_{p|p}|p|p| + K_{\dot{p}}\dot{p} + K_{prop} + K_{HS}$$

$$\sum M = M_{w|w}|w|w| + M_{wp}wp + M_{rp}rp + M_{\dot{w}}\dot{w} + M_{vp}vp + M_{\dot{q}}\dot{q} + M_{q|q}|q|q| + M_{uq}uq + M_{uu\delta_s}u^2\delta_s + M_{HS}$$

$$\sum N = N_{v|v}|v|v| + N_{wp}wp + N_{ur}ur + N_{\dot{v}}\dot{v} + N_{pq}pq + N_{\dot{r}}\dot{r} + N_{r|r}|r|r| + N_{uv}uv + N_{uu\delta_r}u^2\delta_r + N_{HS}$$

Parameter values and their definitions can be found on Prestero [37].